Mapping aerial metal deposition in metropolitan areas from tree bark: a case study in Sheffield, England

E. Schelle[a], B. G. Rawlins[*,b], R. M. Lark[c], R. Webster[c], I. Staton[a], C. W. Mcleod[*,a]

[a] *Centre for Analytical Sciences, Department of Chemistry, University of Sheffield, Sheffield S3 7RF, UK*

[b] *British Geological Survey, Keyworth, Nottingham NG12 5GG, UK*

[c] *Rothamsted Research, Harpenden, Hertfordshire AL5 2JQ, UK*

[*] Corresponding authors:

B. G. Rawlins

British Geological Survey

Keyworth

Nottingham NG12 5GG

UK Telephone: +44 (0)

Fax: +44 (0)

e-mail: bgr@bgs.ac.uk

C. W. Mcleod

Centre for Analytical Sciences

Department of Chemistry

University of Sheffield

Dainton Building

Sheffield S3 7HF

UK

Telephone: +44 (0) 114 222 3602

Fax: +44 (0) 114 222 9379

e-mail: c.w.mcleod@sheffield.ac.uk

Abstract

We investigated the use of metals accumulated on tree bark for mapping their deposition across metropolitan Sheffield by sampling 642 trees of three common species. Mean concentrations of metals were generally an order of magnitude greater than in samples from a remote uncontaminated site. We found trivially small differences among tree species with respect to metal concentrations on bark, and in subsequent statistical analyses did not discriminate between them. We mapped the concentrations of As, Cd and Ni by lognormal universal kriging using parameters estimated by residual maximum likelihood (REML). The concentrations of Ni and Cd were greatest close to a large steel works, their probable source, and declined markedly within 500 metres of it and from there more gradually over several kilometres. Arsenic was much more evenly distributed, probably as a result of locally mined coal burned in domestic fires for many years. Tree bark seems to integrate airborne pollution over time, and our findings show that sampling and analysing it are cost-effective means of mapping and identifying sources.

Capsule: Multi-element analysis of tree bark can be effective for mapping the deposition of metals from air and relating it to sources of emission.

Keywords: Multi-element analysis; Arsenic; Cadmium; Nickel; Geostatistics; REML; Universal kriging

1. Introduction

Inhalation of atmospheric aerosols, particularly of the fine size-fraction, can cause lung diseases, and regulatory standards exist to ensure that air quality meets internationally defined standards. Airborne particulate matter (APM) for $PM_{2.5}$ and PM_{10} is now widely monitored, particularly in urban environments. Nevertheless, government agencies and local authorities rarely have the resources to install equipment at the many sites that would be needed to map the spatial distribution of airborne particles. Normal practice for monitoring metals in APM is to establish installations at a few fixed locations, as in the Heavy Metals Monitoring Networks in the United Kingdom (Brown et al., 2007).

Typical of this approach is the study of Moreno et al. (2004) who analysed APM at five sites in England and Wales. They showed that the air in Sheffield contained many metal-bearing particles in the $<PM_{2.5}$ size-fraction. Those containing Cd and Ni are likely to derive from large steel works (Buse et al., 2003) and to impair health when inhaled. Attempts to apportion the particles to particular sources of metals in APM include chemical mass balance (Wang et al., 2006; Samara et al., 2003) and multivariate statistical analyses (Kim et al., 2006; Shah et al., 2006). Thomaidis et al. (2003) incorporated meteorological variables in their multivariate analysis because they found these influenced the concentrations of Cd, Ni and As in the APM in Athens. Sweet and Vermette (1993) studied anthropogenic emissions in urban Illinois based on trace metal data from three sites; they reported much temporal variation in the quantity of metal in the APM. They attributed this to variations in wind strength and direction, and the degree of atmospheric mixing. Atmospheric particulate matter in towns and cities is readily resuspended, and this process contributes significantly to temporal (Vermette et al., 1991) and spatial variation in the contents of metals (Kuang et al., 2004). So mapping the spatial distribution from direct measurements would require many permanent sampling installations to integrate concentrations over

time.

An attractive approach for mapping the long-term spatial distribution of elements in APM is by biomonitoring. The underlying idea is to let plants accumulate atmospheric depositions over time and then to analyse chemically the plant tissue. The scope for exploiting plants in this way is diverse and includes plant leaves, lichens, mosses and tree bark (Markert et al, 1993; Walkenhorst et al. 1993). The outer layer of tree bark, in particular, has been found to be an effective passive accumulator of airborne particles in both rural (Bohm et al., 1998) and urban (Tanaka and Ichikuni, 1982) environments. The particles in question settle on the outer bark by wet and dry deposition, and they remain there until the tree sheds its bark, or are leached or washed away by rain, or a combination of the two.

Smooth-barked trees in the northern temperate zone begin to shed their bark only when mature (after about 50 years); trees with rougher bark tend to shed theirs somewhat earlier. The metal species deposited in the outer bark are separated physically from trace elements taken up in solution from the soil in the trees and their xylem by a layer of phloem and cambium (Martin and Coughtrey, 1982). Further, extraneous contamination from the soil itself is limited to lowest 1.5 m of the trunk. So pollutants in the bark above this height are almost entirely derived from the air (Wolterbeek and Bode, 1995).

Determination of the metal contents of tree bark cannot lead to a direct assessment of air quality because such measurements are retrospective and integrate as averages over long times. Nevertheless, because trees are widespread in most towns and cities, sampling their bark for subsequent chemical analysis and then noting precise locations mean that the elemental concentrations in the barks can be mapped. Such maps, whether simple displays of measured concentrations or ones made by more elaborate interpolation could point to the emitter(s) of the metals, and identify regions where much (and little) metal is deposited. To date there have been few published attempts to map the distributions of metals from the analysis of tree bark. One was by

Lotschert and Kohm (1978) who drew isarithmic ('contour') maps of Pb and Cd based on samples from 34 ash trees (*Fraxinus excelsior*) throughout Frankfurt. A similar approach, adopted by Bellis et al. (2001) to map airborne emissions in the vicinity of a lead smelter, was based on plotting data on the enrichment in Pb. On a national scale Lippo et al. (1995) drew a 'pollution' map of Finland detailing anthropogenic emissions for cities and industrial regions.

We have investigated the potential of tree bark for mapping the accumulated deposition of airborne metals across metropolitan Sheffield, a city which has more trees per unit of population than any other in Europe. We measured the concentrations of 18 metal and metalloid elements in bark at 642 locations in the region and compared them with those at a virtually uncontaminated site (Mace Head, western Ireland) to determine the magnitude of contamination in the former. We collected bark samples from three tree species to determine whether there were any substantial differences in metal contents between them. We did a principal component analysis on the elements to establish the relationships between the elements and to discover whether there were particular groups of them that might behave differently from one another. We then chose three potentially toxic elements, namely Cd, As and Ni, as representatives and analysed their data spatially (a) to determine regional trends, (b) to estimate their spatial covariances, and (c) to interpolate and map their distributions by kriging. We have used these maps to identify likely local sources of atmospheric pollution. We discuss the wider implications of our findings for the use of tree bark in environmental monitoring.

2. Materials and methods

2.1 Study region, tree bark survey and analysis.

Sheffield has a long tradition of iron smelting and the production of steel. The invention of the crucible process in 1740 sparked a massive expansion of the industry in the city, relying in part on coal from local mines, which continues to this day. This in turn led to

severe air pollution before measures to combat it were introduced under the Clean Air Act of 1956. In 1963 the company British Steel opened a large works at Tinsley in the north east of the city (Figure 1) to make special steels. Its production, including that of stainless steel (ferrochrome), continues and emits significant quantities of Cr and Ni into the atmosphere. Gilbertson et al. (1997) reported on the long-term significance of metal emissions from steel manufacturing from their study of concentrations of Co, Cu, Fe, Ni, Pb, and Zn in a peat monolith from close to the works. They found extraordinarily large concentrations (in mg kg^{-1}) of Cu (472), Ni (320), Pb (827) and Zn (613) compared to concentrations in soil from an urban survey of the city for which Rawlins et al. (2005) presented data for Pb and Ni. The study of Gilbertson et al. attributed the greatest enrichment of Cu and Zn in the uppermost layers to the works.

The Environment Agency of the UK had compiled an inventory of pollution (Environment Agency, 2003) in which it registered the locations and quantities of atmospheric particulate metal emissions from static sources. The inventory included emissions exceeding the reporting thresholds of 100 g for Cd, 1 kg for As and 10 kg for Ni, each per year. It did not include sources of smaller amounts for which no information is available on metal composition. We collated the data for the Sheffield region and to 3 km beyond its boundary for the years for which data were available prior to our collection of the bark samples (1998–2002). We calculated the sum of emissions for the five years so that they could be presented as total emission figures (in kg) for each particular source.

Below we discuss the significance of these sources in relation to the distributions of the metals in bark.

In establishing the region for our current study we wished to encompass the major sources of metal emissions, including industry to the north and east of the City, whilst also estimating the spatial extent of metal deposition. We therefore surveyed an area extending across the city from the suburbs of Whirlow and Greenhill south and west of the centre and from which the prevailing wind blows (see wind rose inset

in Figure 1) to industrial Brinsworth and Ecclesfield to the north-east of the city centre (see Figure 1). The number of people living in the region, estimated from the 1991 census, is approximately 271 500. This figure was calculated from the UK EDINA database of population-weighted centroids defined for all the 1991 enumeration districts (Bracken and Martin, 1989.). The total population of greater Sheffield is around 550 000.

Samples of bark were collected from 642 trees of the three species (with proportions of each shown in parentheses): sycamore (*Acer pseudoplatanus* — 68%), oak (*Quercus robur* — 22%) and cherry (*Prunus serrula* — 10%); their locations are shown in Figure 1. Both sycamore and cherry have fairly smooth bark, whereas the bark of oak is rougher. The samples were collected between April and November, 2003. In a series of local neighbourhoods, trees belonging to the three species occurring in a public space were identified. From these a subset was sampled to provide, as far as possible, an even spatial distribution.

Approximately 10 g of the external outer bark (1–2 mm depth) was removed from each target tree with a clean scraping tool at 1.5 m above the ground. Sample sites spanned an altitude range of 271 m, from 33 to 301 m above mean sea level. The mean altitude was 106 m.

Trees in the temperate zone of the UK enlarge their diameters by approximately 1 cm per year, so a tree's circumference in cm divided by π gives an approximate age of the tree (P. Casey, personal communication). The ages of the trees from which bark was sampled ranged from 25 to 45 years (circumferences of 78 to 141 cm). Bark with moss, lichen or paint was excluded from the sample. The orientation of the location for sampling was random. The samplers wore polythene gloves to avoid contaminating the samples, which were stored in sealed brown paper envelopes at 4 °C. The geographic co-ordinates and altitude of each site were obtained by GPS (Garmin International, Inc., USA). A further nine bark samples were collected from sycamore trees at Mace Head on the west coast of Ireland (53° 20' N, 9° 54' W) so that we could estimate

background concentrations where there is negligible pollution.

Each bark sample was crushed into a fine powder in a Tema mill. The bark powder was then passed through a sieve (0.5 mm mesh) to remove any large lumps. Thereafter all the equipment was cleaned thoroughly to prevent cross-contamination of the following sample. Tree bark powder (4.0 g) was thoroughly mixed with polystyrene co-polymer binder (0.9 g) (Hoechst Wax, Spectro Analytical, UK) and pressed for 1 minute to produce powder pellets. The powder pellets were analysed by EDXRF spectrometry (X-LAB, Spectro Analytical, UK). The instrument was calibrated for 18 elements (Ag, Al, As, Ba, Cd, Co, Cr, Cu, Fe, Mn, Ni, Pb, Sb, Se, Sn, Ti, V, Zn) for a wide range of standard biological reference materials which included poplar leaves, lichen, human hair and tea leaves. Typical analytical performance has been published previously (Schelle et al., 2002). The concentrations of Cd were less than the detection limit for 19% of the samples, and so we set their values to half that limit for subsequent statistical analysis. Fifty two percent of the samples contained less than the detection limit of Ag, and so we do not consider it further.

2.2 Summary statistics

Table 1 summarizes the data for all 17 elements. The distribution of most was positively skewed, some strongly, and so to stabilize variances for subsequent analyses we transformed the values to logarithms. The table lists the transformations we made.

As expected, there is a huge range in the mean values. Aluminium, which is the most abundant metal in the rocks and soil, is most abundant in the bark also. Iron appears in large amounts, and given Sheffield's history we might expect such results too. The concentrations of the other elements do not immediately stand out. With the exception of Al, the mean concentrations in Sheffield were much larger than those those at Mace Head (Table 2); for Cr, Mn, Ni and Ti they were an order of magnitude larger. Anthropogenic sources are almost certainly the reason for the greater concentrations of metal in the tree bark in Sheffield.

What is highly significant is that the distributions of all the elements are strongly

positively skewed, with skewness coefficients ranging from 1.7 to almost 10. We found that all could be described well by a three-parameter log-normal distribution, which has the probability density function:

$$g(z) \;=\; \frac{1}{\sigma(z-\alpha)\sqrt{2\pi}} \exp\left[-\frac{1}{2\sigma^2}\left\{\ln(z-\alpha)-\mu\right\}^2\right] \;, \qquad (1)$$

where z is the variable of interest, μ and σ are the mean and standard deviation of the transformed variable, and α is the shift in the original scale to maximize the goodness of fit. The shift and the mean and standard deviations in natural logarithms are listed in Table 1. In the final column of Table 1 are the skewness coefficients of the logarithms from which it is evident that the transformations have made the distributions symmetric. This is important for stabilizing the variances, and we have done all our further analyses on these transformed scales.

Analysis of variance revealed little differences among species; they accounted for less than 5% of the variance for any of 16 metals and for only 8.5% for As. We have therefore disregarded differences between species in our subsequent multivariate and spatial analysis.

2.3 Selection of variables; principal component analysis.

For the purpose of this paper we wanted to select a few elements from the 17 listed above that would illustrate both the feasibility of analysing APM in bark and mapping the distribution of elements in it and produce maps interesting in their own right. To help in the selection we did a principal component analysis on the correlation matrix of the logarithms. We hoped thereby to see any clusters of strongly correlated elements from which we could choose representatives and any other elements that were clearly uncorrelated with others and should be treated in their own right. Table 3 lists the leading eigenvalues of the correlation matrix. The first component accounts for almost half the variance, and second and third together account for more than half the remainder. Pursuing the analysis, we computed the correlation coefficients, r_{ij},

between the principal component scores and the (logarithms of the) original variables as

$$r_{ij} \;=\; \nu_{ij}\sqrt{\lambda_j/\sigma_i^2}\;, \tag{2}$$

where ν_{ij} is the ith entry in the jth eigenvector, λ_j is the jth eigenvalue, and σ_i^2 is the variance of the ith original variable. We then plotted the results in the unit circles for pairs of the leading components. We show two such circles in Figure 2 in which we have plotted the correlation coefficients (a) for component 2 against component 1 and (b) for component 3 against component 1. In general, the closer the points lie to the circumference of one of these circles the better are they represented in that projection.

We note first that all of the plotted points fall in the right hand halves of the graphs: component 1 is essentially one of size. Component 2 discriminates, separating the siderophile (Fe, Mn, Co, Ni) and lithophile (Cr and V) elements from the calcophile group (Pb and Zn) and their associates. Arsenic appears nearest the centre in circle (a) and the least correlated with the other elements. This is confirmed in circle (b) in which the point for As lies close to the circumference and away from the other elements. Somewhat surprisingly Zn lies near the bottom of axis 3. The siderophiles remain clustered in this projection.

From this examination of the data we have chosen three elements for our spatial analysis. We have chosen Ni as representative of the siderophiles and because it is a key element in steel production. We chose Cd because of its potential toxicity and again used in manufacturing. Third, we chose As, another poison, but from Figure 2(b) clearly dissociated from the other elements.

2.4 Spatial modelling by REML

Our objective is to display the spatial variation of the three selected elements on tree bark across Sheffield as isarithmic ('contour') maps having first estimated the concentrations at the nodes of a fine grid. We used kriging for the estimation, following closely the technique we used to map the distribution of metals emitted from a smelter

and described recently in this Journal (Rawlins et al., 2006).

Ordinary kriging is based on two assumptions.

1. A variable of interest, y, at locations $\mathbf{x}_i$, $i = 1, 2, \ldots$, is a realization of an intrinsically stationary correlated random function $Y(\mathbf{x})$ such that

$$\mathrm{E}\left[Y(\mathbf{x}) - Y(\mathbf{x}+\mathbf{h})\right] \;=\; 0 \quad \text{for all } \; \mathbf{x},\; \mathbf{h}\;, \tag{3}$$

where $\mathrm{E}[\cdot]$ denotes the statistical expectation of the term in brackets, and $\mathbf{h}$ is a lag vector, a displacement in space from the location $\mathbf{x}$.

2. The expected squared difference between $Y(\mathbf{x})$ and $Y(\mathbf{x}+\mathbf{h})$ depends only on $\mathbf{h}$:

$$\mathrm{E}\left[\{Y(\mathbf{x}) - Y(\mathbf{x}+\mathbf{h})\}^2\right] \;=\; 2\gamma(\mathbf{h})\;. \tag{4}$$

The quantity $\gamma(\mathbf{h})$ is the variance perpoint at lag $\mathbf{h}$ and as a function of $\mathbf{h}$ is the variogram.

A preliminary display of the data for Ni and Cd at least suggested that the assumption in Equation (3) was not tenable; there were evident trends from small concentrations far from the steel works in the south west of the city to large ones close to the works in the north east, as we expected. This situation requires more complex geostatistical analysis in which the trend is separated from the random component and the estimates are made by universal kriging (Matheron, 1969), or 'kriging with trend' as it is now more generally known. Saito and Goovaerts (2001) encountered a similar problem in a study on the distribution of metal pollutants in two urban areas in the United States. In each case there were clear trends in the distribution of these contaminants, which could be accounted for by the wind direction and the location of sources (one smelter in one of the areas, and two adjacent smelters in the second). They used this information to produce simple trend models, based on physical principles, which predict the amount of metal that has been deposited from the sources at any location. This constituted the trend in their universal kriging. In order to model the spatial dependence of the random component, the residual from the trend, they

estimated variograms of the pollutant from paired comparisons between sites at which the trend was deemed to be similar. This crudely filters the trend from the variogram that is obtained. It also discards the information about the random component of variation that could be obtained from comparisons between points where the trend is very different. To do this requires a more sophisticated analysis.

Recent developments in numerical analysis linked to modern computing power enable us to use Residual Maximum Likelihood (REML) for the purpose, and we must now regard this as best practice. We described the procedure fully in Rawlins et al. (2006), and we shall not repeat the detail here. In this respect, then, our analysis was more sophisticated than that of Saito and Goovaerts (2001). In another respect it was more primitive, because we did not attempt to use a physically-based model for the trend in metal content of the bark. This was because, by contrast to the two regions studied by Saito and Goovaerts (2001), Sheffield has multiple sources of metal pollutants, and not only current or recent ones, but also many others from the distant past about which we have no detailed information. For our trend models therefore we considered only simple functions of the spatial coordinates.

We treat the transformed data as the outcome from a mixed model:

$$Y(\mathbf{x}) \;=\; \sum_{k=0}^{K} \beta_k f_k(\mathbf{x}) + \varepsilon(\mathbf{x}) \;. \tag{5}$$

It consists of $K+1$ fixed effects (which explain the trend in terms of known functions of the spatial co-ordinates) and a spatially dependent random variable $\varepsilon(\mathbf{x})$ with mean zero and variogram $\gamma(\mathbf{h})$. In order to apply REML to estimate the variance of the random variable and its spatial dependence we make stronger assumptions of stationarity than the intrinsic hypothesis stated in Equations (3) and (4) above. We require that the random variable is second-order stationary, which means that the variogram is bounded by the *a priori* variance of the process. This is not a serious constraint in practice once we have separated out the fixed effects, and is met by most of the popular variogram models used in geostatistics. Our task is to estimate the contributions of the fixed and random components simultaneously, minimizing the estimation variance.

The separate contributions need not be explicitly computed when we use universal kriging, but they should be inspected to assess the weight of evidence for a trend in the variable.

We first chose a few plausible models for the trend in Equation (5) by inspection of the data. We then separated these trends from the data and computed experimental variograms of the residuals by the usual method of moments:

$$\widehat{\gamma}(\mathbf{h}) \;=\; \frac{1}{2m(\mathbf{h})} \sum_{j=1}^{m(\mathbf{h})} \{y(\mathbf{x}_j) - y(\mathbf{x}_j + \mathbf{h})\}^2 \;, \tag{6}$$

where $y(\mathbf{x}_j)$ and $y(\mathbf{x}_j+\mathbf{h})$ are the values of y at sampling points $\mathbf{x}_j$ and $\mathbf{x}_j+\mathbf{h}$ separated by the lag $\mathbf{h}$ and $m(\mathbf{h})$ is the number of paired comparisons at that lag. We fitted several of the standard simple models to these variograms by weighted least squares and chose the ones that fitted best in the least squares sense.

This estimation of the trend ignores the spatial correlation of the residuals, but is acceptable for exploratory purposes. We found that we could describe the trend in the transformed data simply by the distance from a reference site in the north-east of the region, so that our full model for the variation was

$$Y(\mathbf{x}) \;=\; \beta_0 + \beta_1 ||\mathbf{x} - \mathbf{x}_\mathrm{R}|| + \varepsilon(\mathbf{x}) \;, \tag{7}$$

where $||\cdot||$ denotes the Euclidean norm of the enclosed vector. The vector $\mathbf{x}_\mathrm{R}$ is the reference site close to the steel works in the north-east of the region with British National Grid co-ordinates (441945.8, 390339.4). We chose this model in preference to a more conventional linear function of the co-ordinates because it achieved at least as good an ordinary least-squares fit to the data with one fewer terms.

We then computed the experimental variograms of the ordinary least-squares residuals and found that an isotropic exponential model with nugget gave a satisfactory fit. Its equation is

$$\gamma(h) \;=\; c_0 + c\left\{1 - \exp\left(-\frac{h}{a}\right)\right\} \;, \tag{8}$$

in which c_0 is the nugget variance, c is the sill of the correlated variance, a is a distance parameter and $h = ||\mathbf{h}||$ is now a scalar in distance only. This model, which is widely

used in geostatistics, increases asymptotically to its maximum, with an effective range of $3 \times a$.

We then used the ASREML program (Gilmour et al., 2002) to fit the model in Equation (7) to each variable. We specified an exponential correlation function, which corresponds to the exponential variogram in Equation (8). The program provides REML estimates of the parameters c_0, c and a, and generalized least-squares estimates of the fixed effects. We tested the null hypothesis that the true value of the fixed effect for the trend, β_1, is zero by computing the Wald statistic. This statistic is equivalent to the variance ratio for the predictor in an analysis of variance for an ordinary least-squares regression. However, we used the method of Kenward and Roger (1997) to compute an adjusted Wald statistic, and adjusted degrees of freedom in the denominator for the F test to allow for the spatial dependence of the residuals.

2.5 Lognormal universal kriging

For reasons described above we transformed the raw data, $z(\mathbf{x})$, to approximately normally distributed variables, which we have denoted by $y(\mathbf{x})$. These values were used to obtain predictions at points on a fine grid over the region by universal kriging. The universal kriging (UK) uses the specified fixed effects in the prediction and the covariance parameters estimated by REML. Note that for arsenic, for which the trend was effectively constant, the universal kriging predictions are the same as those from ordinary kriging since we estimate one fixed effect, β_0, which is the mean.

Universal kriging returns an estimate of the transformed random variable $Y(\mathbf{x})$; but we require estimates on the scale of the original data $z(\mathbf{x})$. As with any estimate derived from log-transformed data, we cannot simply back transform the estimates on the logarithmic scale; we must also correct for bias. Cressie (2006) has shown that the UK estimate of a log-normal variable $\tilde{Z}'(\mathbf{x}_0)$, based on the UK estimate $\tilde{Y}(\mathbf{x}_0)$ of the corresponding Y, is

$$\tilde{Z}'(\mathbf{x}_0) \;=\; \exp\left\{\tilde{Y}(\mathbf{x}_0) + \frac{1}{2}\sigma^2_{\mathrm{UK}} - \psi_0 - \sum_{i=1}^{K}\psi_i f_i(\mathbf{x}_0)\right\}\;, \tag{9}$$

where the $\psi_0, \psi_1, \ldots$ are Lagrange parameters from the UK system (see Rawlins et al., 2006). We therefore back-transformed our kriged estimates in this way.

We kriged the log-transformed variables at the nodes of a 200-m square grid. For each variable we specified the fixed effects selected after the REML analysis, and the covariance parameters obtained from that analysis. All observations were used for kriging at all target sites because we wanted the trend model at all target sites to be the same as the overall trend model to which our variogram refers. Since the number of data is large, this could lead to difficulties with the inversion of a large matrix. Our program for obtaining the lognormal UK estimates uses a subroutine for matrix inversion (LINRG, from IMSL, Visual Numerics, 1997) that reports any conditioning problems. It did not do so. We then used Equation (9) to transform the estimates back to the original scale, and corrected for the shift constant, α, in the original log-transformation. A particular advantage of kriging, relative to other methods for spatial prediction such as arbitrarily weighted local averaging, is that the error variances of the predictions are minimized and also (generally) is known. Unfortunately, back-transformations of the variances in the logarithms to the original scale can be calculated only for the simple kriging case (Webster and Oliver, 2007). Nevertheless, because we know the prediction variances on the transformed scale we can compute confidence limits and transform them. This therefore is what we did; we computed the local 95% upper limits in the logarithms and transformed them to the original scale of measurement.

3. Results and their interpretation

3.1 Trend and variance models based on REML

As above, we analysed the data for the three elements Ni, Cd and As. Their histograms appear in the top row of Figure 3 and are evidently strongly positively skewed. The middle row of histograms in the figure are of their logarithms; the transformation has conferred symmetry (see also Table 1) and left no outliers. Finally, in the bottom row

of the figure are the histograms of the residuals of the transformed data of Ni and Cd from their trends. Again the residuals for Ni and Cd are symmetrically distributed with small coefficients of skewness (-0.17 and 0.03 respectively). This gives us confidence that the assumption of normality of the random process, implicit in our use of REML for estimation of the variance model, is plausible. They show that, under the logarithmic transform, our data contain no obvious marginal outliers that might distort the variance model or local estimates. Finally, they show that the residual variation has been diminished—the standard deviation of the residuals of Ni is 0.794 compared with 1.202 in the logarithms and that of Cd is 0.796 compared with 1.091.

The trend models fitted for each element, after log-transformation, are listed in Table 4. Note that for both nickel and cadmium the estimated coefficient β_1 is negative, and that the null hypothesis that there is no trend can be rejected decisively because of the very small value of P in the Wald test. The negative coefficient implies that the larger concentrations of metals are near the reference site in the north-east of the region. All the registered sources of Ni and Cd emissions occur in the north-east of the region also. The source with the largest emission of Ni (having emitted a total of 10 800 kg from 1998 to 2002) by almost one order of magnitude is 2.6 km to the west of the reference site (Figure 4a). The same emitter was also the largest source of Cd (having emitted 227 kg over the same period; Figure 4b). When the wind blows from the north and east these metals are dispersed towards the south and west, accounting for the observed trend. We do not observe the same degree of trend in the pattern to the north and east because when the wind blows from the south and west — the dominant prevailaing direction — significant quantities of metals are deposited towards the northern and eastern boundaries of the study region, where the concentrations remain substantially greater than the near background values observed elsewhere.

The analysis reveals that the random effect for both Cd and Ni has marked spatial dependence; more than half of their variances is spatially correlated to distances

between 2 and 2.5 km. This suggests that there are factors causing this variation unexplained by the trend model and that it might be worth attempting to identify them. The largest concentrations of Ni and Cd occur close to their dominant sources, accounting for the spatial dependence at short distances (Figure 4a and b).

In contrast, there was no evident spatial trend in the concentrations of arsenic, which is confirmed in the formal Wald test of the null hypothesis that β_1 is zero. For this reason we computed a variance model for log-transformed arsenic with only one fixed effect, namely the mean. The variogram parameters for this model were used for the kriging prediction. Note that little more than a fifth of the variance is spatially correlated, and that to distances of approximately only 1.5 km.

3.2 Maps of metal concentration in bark.

Figure 4a shows much short-range variation of Ni in the north-east of the region, which we presume to result from emissions and deposition from both current steel works and ones now defunct over many years. This pattern and the mechanism accord with what we know of total soil Ni concentrations across the city from a recent geochemical survey (Rawlins et al., 2005). The Ni is most concentrated immediately to the west of the big steel works at Tinsley (440 km east, 390 km north; Figure 4a). Another smaller source (437 km east, 389 km north) might account for the large concentrations (400 mg kg^{-1}) in its vicinity and to the north and east in the direction of the prevailing wind. There are two small areas with large Ni values (440 km east, 388 km north; 438 km east, 387.5 km north) which, according to our database, do not have significant sources nearby. Nevertheless, there are within 500 m of these two locations industries that might emit Ni-bearing particles. Concentrations of Ni are generally small in the north and south-west the region where there are no recorded sources of pollution. This suggests that there is little long-range dispersal, resuspension and deposition of the metal.

Let us now turn to Cd. Figure 4b shows the largest concentrations around two sources (437 km east, 388 km north), one where metal is produced and processed

(having emitted a total of 69 kg from 1998 to 2002), the other an incinerator (having emitted 52 kg over the same period). Somewhat surprisingly, the concentrations are smaller near to the source of the largest emission (total emission 227 kg from 1998 to 2002). As with Ni, the concentrations of Cd diminish rapidly within 500 m of these sources, with the larger values extending northeastwards. The spatial patterns of Cd concentrations alone do not appear to reflect the magnitude of local sources, but the temporally varying dispersal mechanisms which depend on the strength and direction of the wind and the height of the emissions. A single spatial outlier with a large concentration of Cd (21.1 mg kg^{-1}) occurs to the south-west of the region (432 km east, 384 km north) in an entirely residential area, and we cannot explain it.

The spatial distribution of arsenic (As) is considerably more complex than that of Ni and Cd. The largest As concentrations do not occur around the steelworks at Tinsley — the largest static emitter (Figure 4c) — but where there are no registered emissions of As (438 km east, 390 km north). This part of the region contains a mixture of residential housing, industry and recreation grounds. Fugitive emissions from the industrial sites could acccount for some of the arsenic. The concentrations diminish rapidly in their immediate vicinity, but more slowly at greater distances. A similar pattern is observed around another area of large concentrations (434 km east, 385 km north), where once again there are no registered sources of emissions and land use is dominantly residential. Arsenic is richer in coal from Sheffield (Yorkshire) than in coal from most other parts of Great Britain. From an analysis of 24 samples of coal from across the country, those from the two Yorkshire seams had As concentrations of 8.7 and 37 mg kg^{-1}, which equate to the 65th and 97th percentile of the As distribution (Spears and Zheng, 1999). Coal was mined and burnt in the City for at least 200 years before the last coal mine was closed and the Clean Air acts were implemented in the 1960s. There would have been many local emitters of As, and the APM from those days might still be being resuspended and redistributed.

4. Discussion

The substantially larger mean concentrations of metals in tree bark across Sheffield than those at Mace Head indicate that most of the metal in Sheffield is of anthropogenic origin. We have also shown that differences between tree species, and any differences in the roughness of their bark, are unlikely to be significant in determining the concentrations of most metals. It should therefore be possible to use tree bark from other species in similar environmental biomonitoring studies without introducing significant error. This is likely to be advantageous where trees of any one species are sparse.

The concentrations of Ni and Cd in the bark of trees in Sheffield show that aerial deposition of metal, and any subsequent resuspension, diminishes markedly within 500 metres of the emitters, though there appears to be significant dispersal over several kilometres. This strengthens the case for biomonitoring of long-term atmospheric pollution via the analysis of tree bark in a cost-effective way and for identifying where the sources of pollution are.

The marked autocorrelation observed in the spatial distributions of Cd and Ni (and also Cr, Co and Cu which we have not described here) indicates that measurements of metals in tree bark in industrial environments can be used to map long-term deposition of those metals from the atmosphere. By contrast, elements such as lead with widespread and even mobile sources, as from motor vehicles before lead was forbidden in fuel in the year 2000, are not spatially correlated; their variograms are wholly nugget at the working scale and so interpolation by any means should not be attempted.

The method we describe and have applied is entirely statistical, though underlain by general knowledge and understanding. We did not attempt to use a source-oriented chemical transport model. We recognize that incorporation of such a model could improve spatial predictions and aid our interpretation of the spatial patterns observed. That is the next logical step in our investigation of these data, and we plan to incorporate such in formation into the linear mixed model that we have used here (see Stacey et al., 2007).

Acknowledgements

This paper is published with the permission of the Director of the British Geological Survey (Natural Environment Research Council). Elvio Schelle is grateful to the Universidade Federal de Mato Grosso (Chiaba, Brazil) for the funding to undertake his PhD study. R.M. Lark's contribution was supported by the Biotechnology and Biological Sciences Research Council of the United Kingdom through its core strategic grant to Rothamsted Research. We thank Colin Powlesland and Alex Hole of the UK's Environment Agency for providing data from the Pollution Inventory.

References

Bellis, D., Cox, A.J., Staton, I., McLeod, C.W., Satake, K., 2001. Mapping airborne lead contamination near a metals smelter in Derbyshire, UK: spatial variation of Pb concentration and 'enrichment factor' for tree bark. Journal of Environmental Monitoring 3, 512–514.

Bohm, P., Wolterbeek, H., Verburg, T. Musilek, L., 1998. The use of tree bark for environmental pollution monitoring in the Czech Republic. Environmental Pollution 102, 243–250.

Brown, R. J. C., Williams, M., Butterfield, D. M., Yardley, R. E., Muhunthan, D., Goddard, S. 2007. Annual Report for 2006 on the UK Heavy Metals Monitoring Network. National Physical Laboratory Report DQL-AS 036. http://www.airquality.co.uk/archive/reports/cat13/0703280922_FINAL_Defra_UK_Heavy_Metals_Network_Annual_Report_2006.pdf. Accessed 1st October 2007.

Bracken, I. Martin, D., 1989. The generation of spatial population distributions from census centroid data. Environment and Planning A 21, 537–543.

Buse, A., Norris, D., Harmens, H., Bker, P., Ashenden, T., Mills, G., 2003. Heavy

metals in European mosses: 2000/2001 survey. http://icpvegetation.ceh.ac.uk/metals_report_pdf.htm. Accessed 14th September 2007.

Cressie, N., 2006. Block kriging for lognormal spatial processes. Mathematical Geology 38, 413–443.

Environment Agency, 2003. Environment Agency Pollution Inventory. http://maps.environment-agency.gov.uk/wiyby/dataSearchController topic=pollution&lang=. Accessed 4th December 2003.

Gilbertson, D.D., Grattan, J.P., Cressey, M. Pyatt, F.B., 1997. An air-pollution history of metallurgical innovation in iron- and steel-making: A geochemical archive of Sheffield. Water, Air and Soil Pollution 100, 327–341.

Gilmour, A.R., Gogel, B.J., Cullis, B.R., Welham, S.J., Thompson, R. 2002. ASReml User Guide, Release 1.0. VSN International, Hemel Hempstead

Kenward, M.G., Roger, J.H. 1997. Small sample inference for fixed effects from restricted maximum likelihood. Biometrics 53, 983–997.

Kim, M.K., Jo, W.K., 2006. Elemental composition and source characterization of airborne PM10 at residences with relative proximities to metal–industrial complex. International Archives of Occupational and Environmental Health 80, 40–50.

Kuang, C., Neumann, T., Norra, S., Stuben, D., 2004. Land use-related chemical composition of street sediments in Beijing. Environmental Science and Pollution Research 11, 73–83.

Lippo, H., Poikolainen, J., Kubin, E. 1995. The use of moss, lichen and pine bark in the nationwide monitoring of atmospheric heavy metal deposition in Finland. Water, Air and Soil Pollution 85, 2241–2246.

528 Lotschert, W., Kohm, H.J., 1978. Characteristics of tree bark as an indicator of
529 high-immission areas: II. Contents of heavy metals. Oecologia 37, 121–132.

530 Markert, B., 1993. Instrumental Analysis of Plants. In: B. Markert (Ed.), Plants as
531 Biomoniots. VCH, Weinheim, pp. 65-103.

532 Martin, M.H., Coughtrey, P.J., 1982. Biological monitoring of heavy metal pollutants.
533 Applied Science Publishers, London.

534 Matheron, G. 1969. Le krigeage universel. Cahiers du Centre de Morphologie
535 Mathématique. Ecole des Mines de Paris, Fontainebleau.

536 Moreno, T., Gibbons, W.,T. Jones, T., Richards, R., 2004. Geochemical and size vari-
537 ations in inhalable UK airborne particles: the limitations of mass measurements.
538 Journal of the Geological Society 161, 899–902.

539 Rawlins, B. G., Lark, R. M., O'Donnell, K.E., Tye, A. M., Lister, T. R., 2005. The
540 assessment of point and diffuse metal pollution from an urban geochemical survey
541 of Sheffield, England. Soil Use and Management 21,353–362.

542 Rawlins, B.G., Lark, R.M., Webster, R., O'Donnell, K.E., 2006. The use of soil
543 survey data to determine the magnitude and extent of historic metal deposition
544 related to atmospheric smelter emissions across Humberside, UK. Environmental
545 Pollution 143, 416–426.

546 Samara, C., Kouimtzis, T., Tsitouridou, R., Kanias, G., Simeonov, V., 2003. Chemi-
547 cal mass balance source apportionment of PM10 in an industrialized urban area
548 of Northern Greece. Atmospheric Environment 37, 41–54.

549 Saito, H., Goovaerts, P., 2001. Accounting for source location and transport direction
550 in geostatistical prediction of contaminants. Environmental Science and Tech-
551 nology 35, 4823–4829.

552 Schelle, E., Staton, I., Clarkson, P.J., Bellis, D.J. McLeod, C., 2002. Rapid multiele-
553 ment analysis of tree bark by EDXRF. International Journal of Environmental
554 Analytical Chemistry 82, 785–793.

555 Shah, M.H., Shaheen, N.N., Jaffar, M., 2006. Characterization, source identification
556 and apportionment of selected metals in TSP in an urban atmosphere. Environ-
557 mental Monitoring and Assessment 114, 573–587.

558 Stacey, K. F., Lark, R.M., Whitmore, A.P., Milne, A.E., 2007. Using a process model
559 and regression kriging to improve predictions of nitrous oxide emissions from soil.
560 Geoderma 135, 107–117.

561 Spears, D.A., Zheng, Y., 1999. Geochemistry and origin of elements in some UK
562 coals. International Journal of Coal Geology 38, 161–179.

563 Sweet, C.W., Vermette, S.J., Landsberger, S., 1993. Soures of toxic trace elements in
564 urban air in Illinois. Environmental Science and Technology 27, 2502–2510.

565 Tanaka, J. Ichikuni, M., 1982. Monitoring of heavy metals in airborne particles by
566 using bark samples of Japanese cedar collected from the metropolitan region of
567 Japan. Atmospheric Environment 16, 2105–2108.

568 Thomaidis, N.S., Bakeas, E.B., Siskos, P.A., 2003. Characterization of lead, cad-
569 mium, arsenic and nickel in PM2.5 particles in the Athens atmosphere, Greece.
570 Chemosphere 52, 959–966.

571 Tye, A.M., Hodgkinson, E.S., Rawlins, B.G., 2006. Microscopic and chemical studies
572 of metal particulates in tree bark and attic dust: evidence for historical atmo-
573 spheric smelter emissions, Humberside, UK. Journal of Environmental Monitor-
574 ing 8, 904–912.

575 Vermette, S.J., Irvine, K.N., Drake, J.J., 1991. Temporal variability of the elemental
576 composition in urban street dust. Environmental Monitoring and Assessment 18,
577 69–77.

578 Visual Numerics, 1997. IMSL Math Library. Visual Numerics, Houston, TX.

579 Walkenhorst, A., Hagemeyer, J. Breckle, S.W., 1993. Passive monitoring of airborne
580 pollutants, particularly trace metals, with tree bark. In: B. Markert (Ed.), Plants
581 as Biomonitors. VCH, Weinheim, pp. 523-540.

582 Wang, X.L., Sato, T., Xing, B.S., 2006. Size distribution and anthropogenic sources
583 apportionment of airborne trace metals in Kanazawa, Japan. Chemosphere 65,
584 2440–2448.

585 Webster, R., Oliver, M.A., 2007. Geostatistics for Environmental Scientists, 2nd
586 edition. John Wiley and Sons, Chichester.

587 Wolterbeek, H.T. Bode, P., 1995. Strategies in sampling and sample handling in the
588 context of large-scale plant biomonitoring surveys of trace element air pollution.
589 Science of the Total Environment 176, 33–43.

List of Figures and Captions

Figure 1. Location and species of trees in the region surveyed from which bark was sampled ($n = 642$). Inset: windrose (source: British Meteological Office) showing direction and strength for 84 662 observations at 146 m above mean sea level in Sheffield.

Figure 2. Projections of the correlation between the 17 elements and principal component scores into unit circles for (a) the first and second components, and (b) the first and third components.

Figure 3. Histograms of raw data (top row), of data transformed to their natural logarithms (centre row) and residuals from the trend for log-transformed data for Ni and Cd (bottom row).

Figure 4. Isarithmic maps of (left) concentrations in bark (back-transformed estimate of the conditional expectation) (right) backtransformed upper 95% confidence limit for the conditional expectation. Also shown are the sources of cumulative emissions from 1998 to 2002 in kg for each of the metals: (a) Ni – A(81), B(10800), C(37), D(519), (b) Cd – A(1), B(227), C(0.4), D(0.5), E(69), F(52) and (c) As – A(40), B(1), C(2.7), D(3.4).

Table 1 Means and standard deviations (Std dev.) in mg kg^{-1} of the amounts of 17 elements in the bark dust, and the means and standard deviations of their natural logarithms after a shift of origin—see text.

	Original measurements			Log transforms			
Element	Mean	Std dev.	Skewness	Shift	Mean	Std dev.	Skewness
Al	9484	46461	7.77	45	7.902	1.103	1.18
Ti	421	465	6.24	29.8	5.812	0.760	0.08
V	24.9	17.2	3.60	5.3	5.701	0.861	−0.39
Cr	265	593	9.14	1.1	4.704	1.283	0.15
Mn	280	360	9.01	11.25	5.349	0.767	0.14
Fe	5712	5669	2.44	264.5	8.354	0.827	0.04
Co	2.93	2.467	2.88	0.198	0.916	0.661	0.12
Ni	65.0	141	12.0	0	3.412	1.202	0.06
Cu	47.3	32.5	1.96	4.3	3.779	0.571	0.06
Zn	152	185	8.38	3.4	4.771	0.781	0.24
As	3.65	2.390	1.77	1.130	1.494	0.451	0.02
Se	1.56	0.955	3.32	0.8	0.801	0.359	0.08
Cd	1.401	3.621	9.97	0.02	−0.368	1.091	0.04
Sn	3.19	3.973	3.18	0.12	0.732	0.942	0.14
Sb	23.9	18.47	1.95	6.6	3.270	0.550	0.03
Ba	245	241	4.39	12.6	5.273	0.721	0.14
Pb	226	153	1.69	45	5.457	0.525	0.02

Table 2 Mean concentrations of 17 elements in nine samples of bark dust from Mace Head (Ireland) in mg kg^{-1}. Analyses reported below the limit of detection (LoD) were set to half this value to calculate the mean. Where the calculated mean was less than the LoD we report the mean as less than the LoD.

Element	Al	Ti	V	Cr	Mn	Fe	Co	Ni	
Mean	12702	32.5	<5	4.7	31.5	218	0.8	1.0	
Element	Cu	Zn	As	Se	Cd	Sn	Sb	Ba	Pb
Mean	8.3	37.2	< 0.2	0.8	<0.3	< 0.6	<0.6	38.2	5.1

Table 3 Eigenvalues of the correlation matrix of the 17 elements, and the percentages of the variance and their cumulants.

Order	Eigenvalue	Percentage of variance	Accumulated percentage
1	8.142	47.89	47.89
2	3.353	19.72	67.61
3	1.303	7.66	75.27
4	0.821	4.83	80.10
5	0.687	4.04	84.14
6	0.554	3.26	87.40

Table 4 Results of the REML estimation of trend models for each element (log-transformed), and REML variance model parameters for the model for arsenic with no spatial trend.

Element	Fixed effects		Wald[a] statistic	P value[b]	Estimated covariance parameters		
	β_0	β_1			a/metres	c_0	c
Ni	5.40	-0.277	106.1	0.55×10^{-6}	705	0.348	0.296
Cd	0.500	-0.135	18.9	2.22×10^{-3}	835	0.531	0.298
As	1.54	-0.003	0.11	0.75	558	0.156	0.047
As		-	-	-	502	0.156	0.046

[a] Wald statistic for the fixed effect β_1.

[b] Null hypothesis that $\beta_1 = 0$.

Figure
Click here to download Figure: figs07.pdf

Figure 1

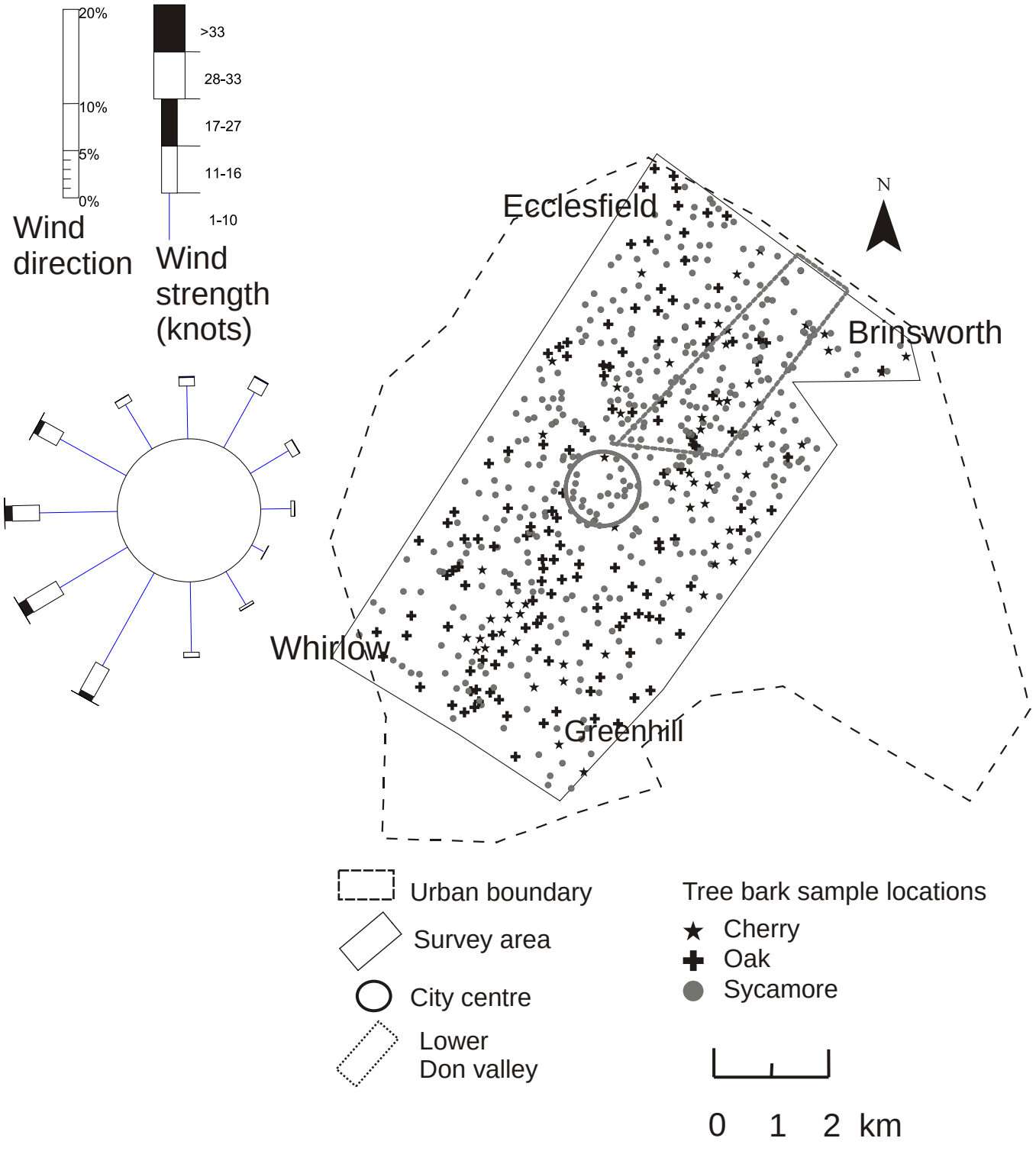

Figure 2

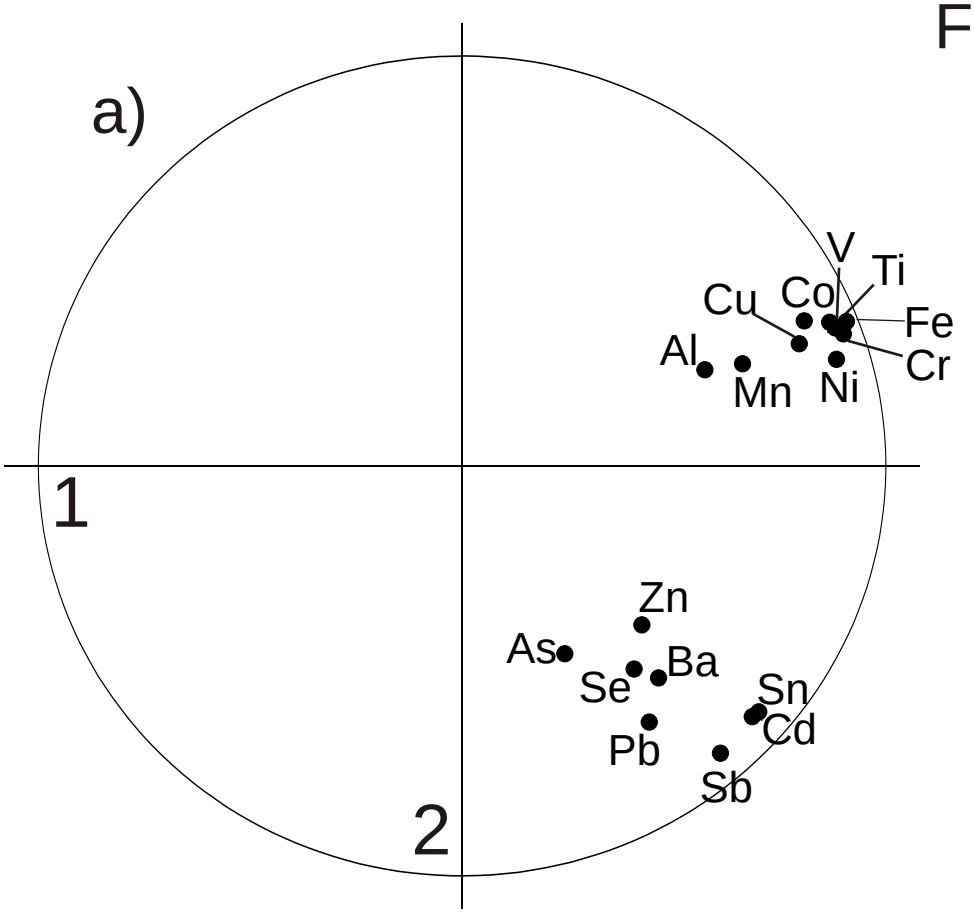
a)
V
Ti
Cu
Co
Fe
Al
Cr
Mn
Ni
1
Zn
As
Ba
Se
Sn
Cd
Pb
Sb
2

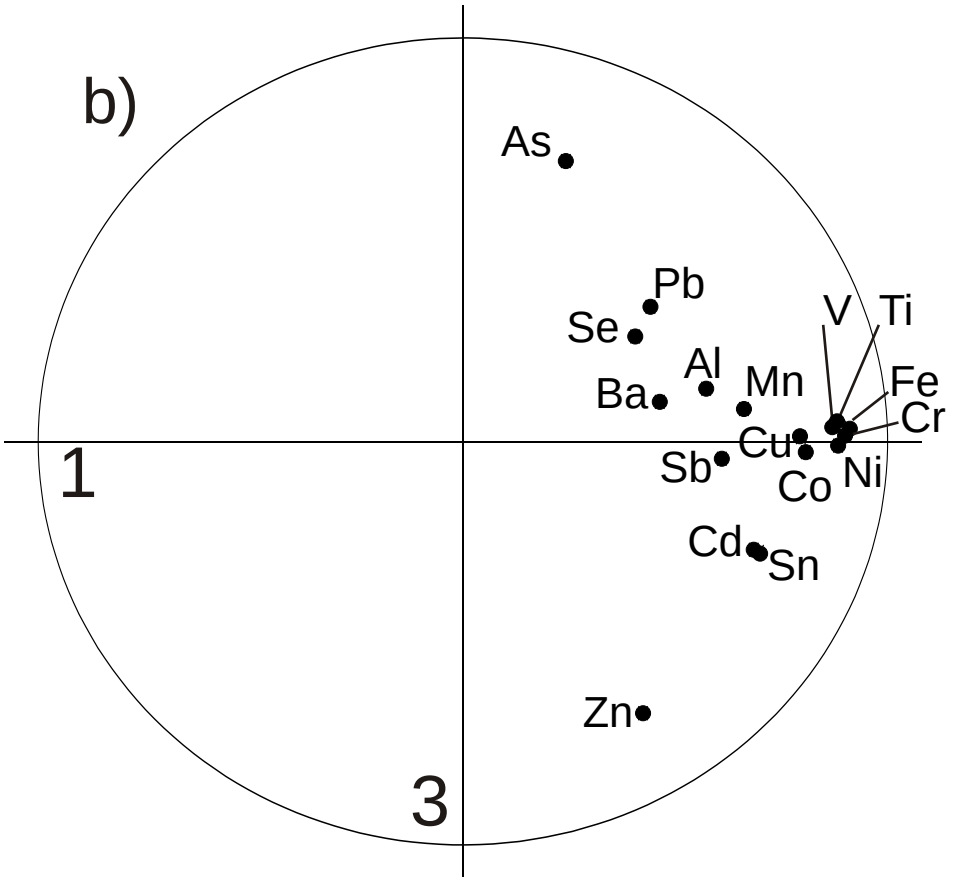
b)
As
Pb
Se
V
Ti
Al
Mn
Fe
Ba
Cr
Cu
Sb
Co
Ni
Cd
Sn
Zn
1
3

Figure 3

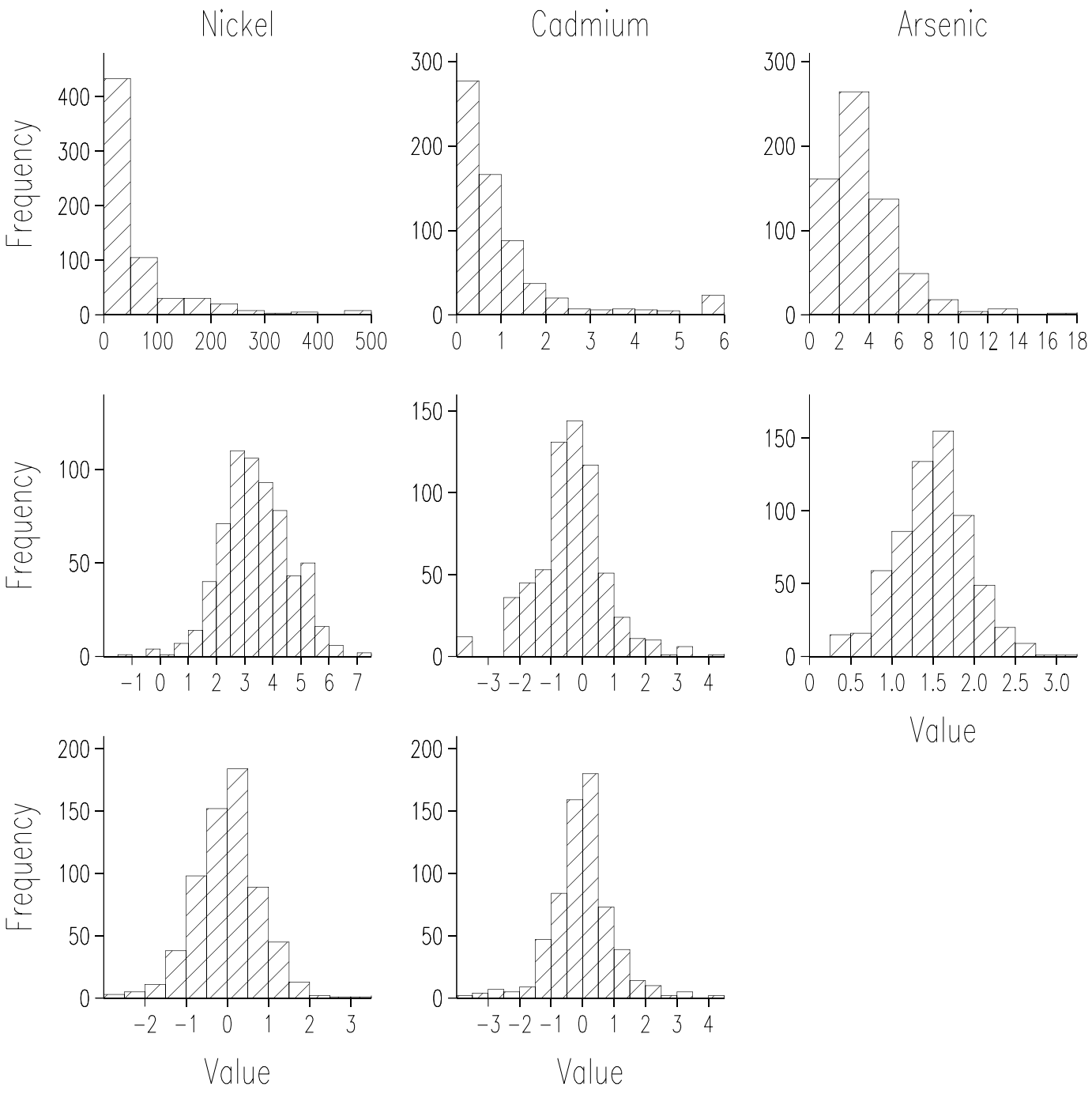
Nickel
Cadmium
Arsenic
Frequency
Frequency
Frequency
Value
Value
Value

Figure 4a

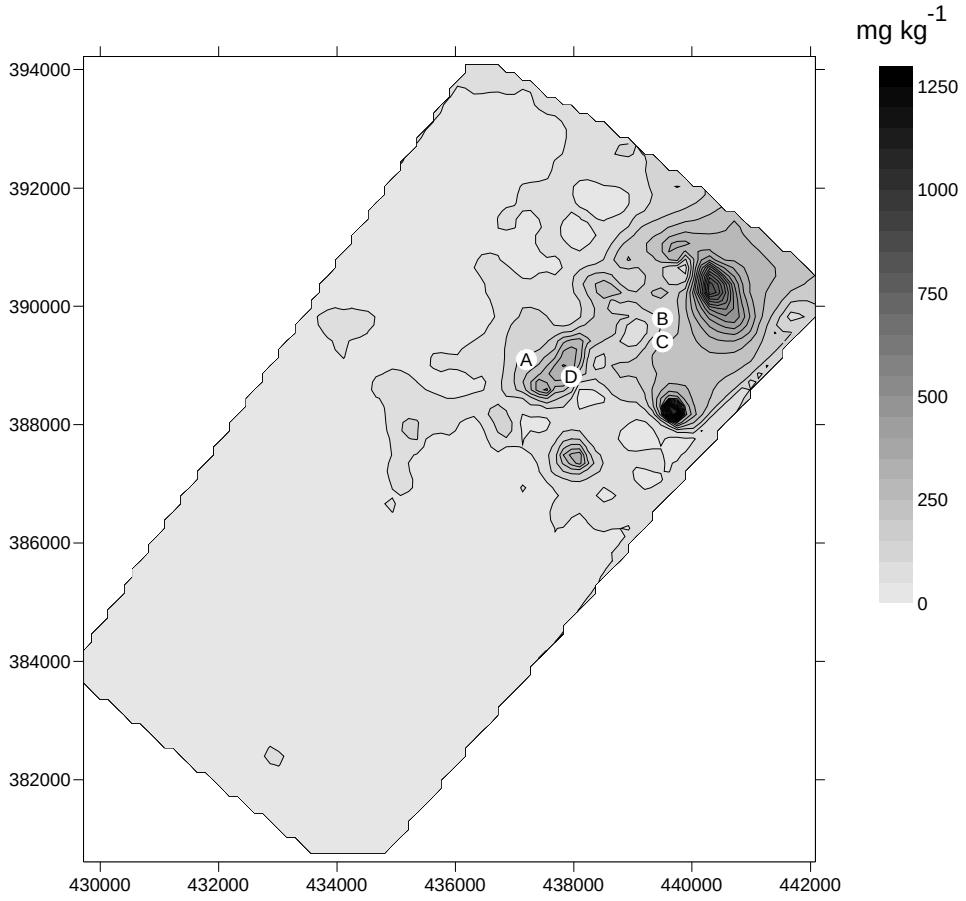
mg kg-1
1250
1000
750
500
250
0
394000
392000
390000
388000
386000
384000
382000
430000
432000
434000
436000
438000
440000
442000
A
B
C
D

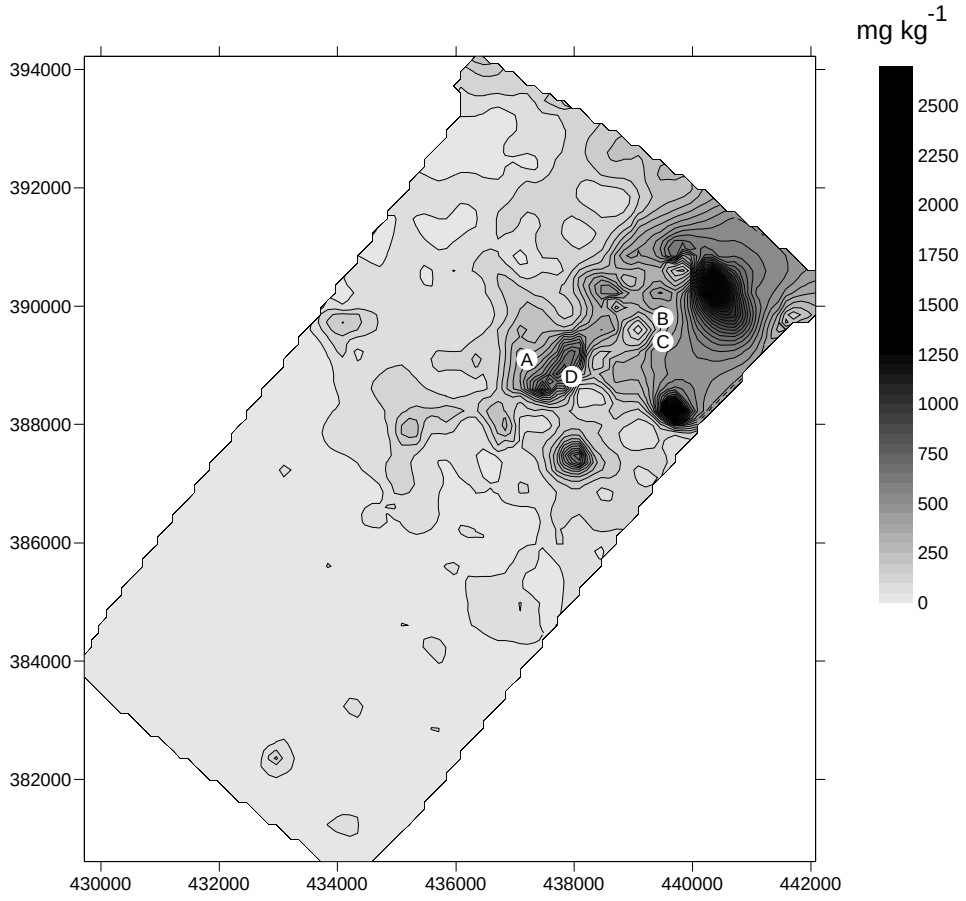
mg kg-1
2500
2250
2000
1750
1500
1250
1000
750
500
250
0
394000
392000
390000
388000
386000
384000
382000
430000
432000
434000
436000
438000
440000
442000
A
B
C
D

Figure 4b

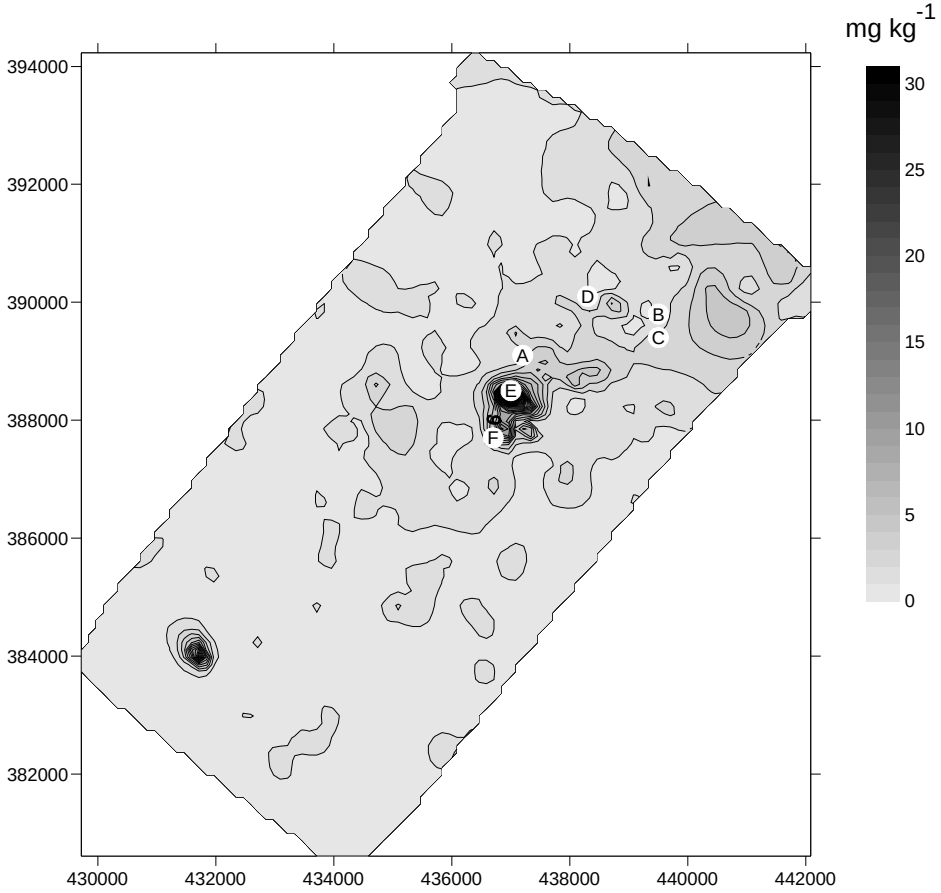
mg kg-1
30
25
20
15
10
5
0
394000
392000
390000
388000
386000
384000
382000
430000
432000
434000
436000
438000
440000
442000
A
B
C
D
E
F

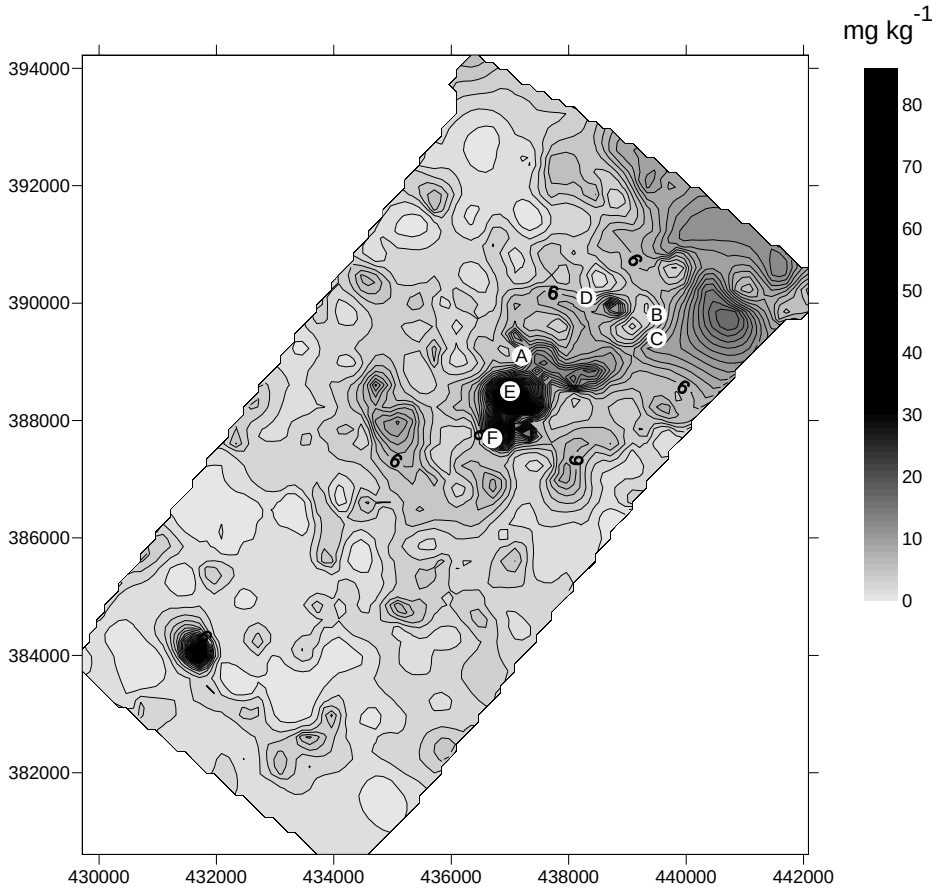
mg kg-1
80
70
60
50
40
30
20
10
0
394000
392000
390000
388000
386000
384000
382000
430000
432000
434000
436000
438000
440000
442000
A
B
C
D
E
F

Figure 4c

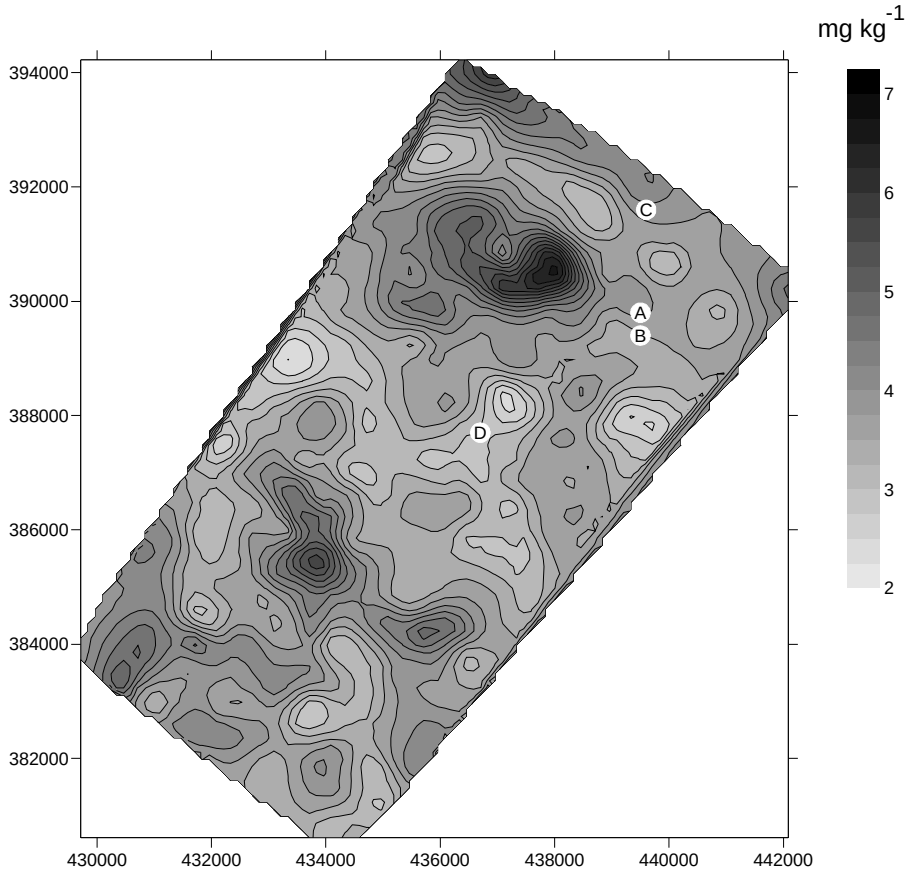
mg kg-1
7
6
5
4
3
2
394000
392000
390000
388000
386000
384000
382000
430000
432000
434000
436000
438000
440000
442000
A
B
C
D

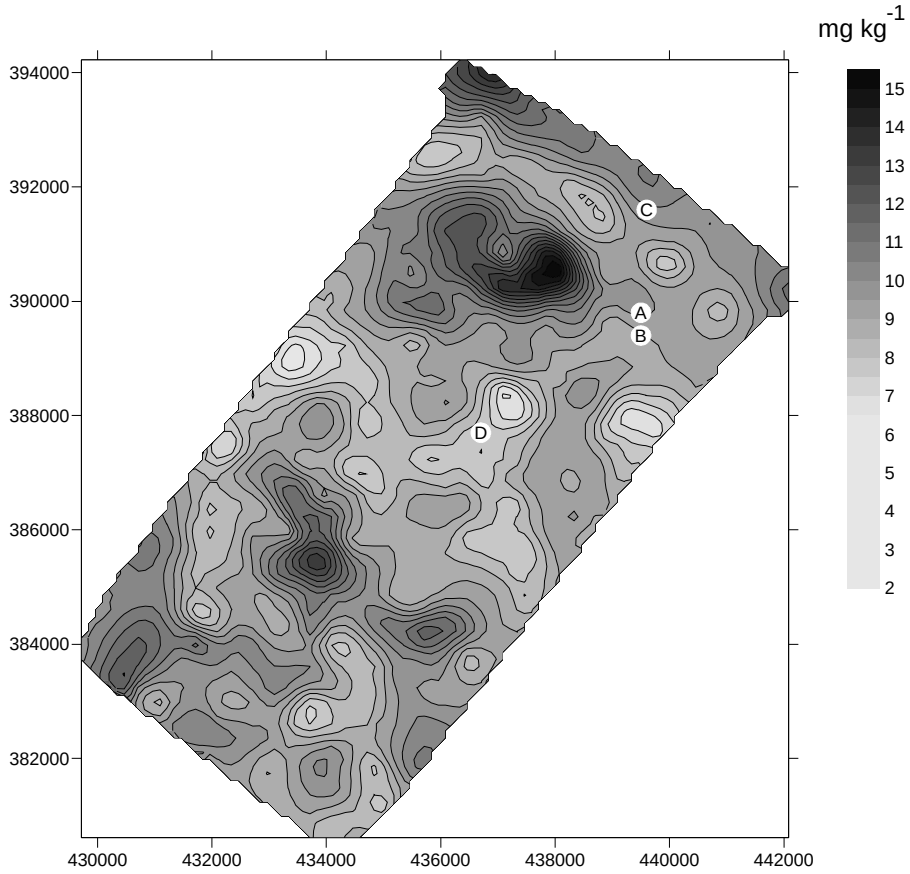
mg kg-1
15
14
13
12
11
10
9
8
7
6
5
4
3
2
394000
392000
390000
388000
386000
384000
382000
430000
432000
434000
436000
438000
440000
442000
A
B
C
D